Received: 28 January 2021 | Revised: 21 May 2021 | Accepted: 27 June 2021

DOI: 10.1002/jbm.b.34914

RESEARCH ARTICLE

Retinoic acid-conjugated chitosan/manganese porphyrin ionic-complex nanoparticles for improved T_1 contrast MR imaging of hepatic fibrosis

Hoa Phuong Tran[1,2] | Yixin Jiang[1,2] | Phuong Hong Nguyen[1,2,3] | Jung Joo Kim[1] | Su-Geun Yang[1,2]

[1]Department of Biomedical Science, BK21 FOUR Program in Biomedical Science and Engineering, Inha University College of Medicine, Incheon, South Korea

[2]Inha Institute of Aerospace Medicine, Inha University College of Medicine, Incheon, South Korea

[3]Institute of Research and Development, Duy Tan University, Da Nang, Vietnam

Correspondence
Su-Geun Yang, Department of Biomedical Science, Inha University College of Medicine, 366, Seohae-Daero, Jung-Gu, Incheon 22332, South Korea.
Email: sugeun.yang@inha.ac.kr

Funding information
National Research Foundation, Grant/Award Numbers: 2019M3E5D1A02069623, 2018R1A6A1A03025523, 2020R1A2B5B02002377

Abstract

Noninvasive and precise diagnosis of hepatic fibrosis is very important for the preventive therapeutic regimen of hepatic cirrhosis and cancer. In this study, we fabricated T_1 contrast Mn-porphyrin ($MnTPPS_4$)/retinoic acid-chitosan ionic-complex nanoparticles (MRC NPs). The functional properties of MRC NPs were evaluated via transmission electron microscopy (TEM) imaging, release study, cytotoxicity assay, hepatocyte-specific uptake assay, and magnetic resonance (MR) imaging study. TEM images confirmed the typical structure of an ionic-complex NPs with around 100–200 nm of diameter. $MnTPPS_4$ is released from MRC NPs for up to 24 hr in controlled pattern which implies that more reliable and convenient hepatic MR imaging is possible using of MRC NPs in clinical practice. Hepatocytes uptake assay proved retinoic acid-specific targeting of MRC NPs. The same results were observed in animal pharmacokinetic studies. In vitro MR phantom study, MRC NPs showed an increased T_1 relaxivity ($r_1 = 6.772\ mM^{-1}\ s^{-1}$) in comparison with $3.242\ mM^{-1}\ s^{-1}$ of $MnTPPS_4$. The result was confirmed again in vivo MR imaging studies. Taken together, MRC NPs displayed a potential for noninvasive diagnostic T_1 MR imaging of hepatic fibrosis with improved target specificity and prolonged MR imaging time window.

KEYWORDS
chitosan nanoparticles, hepatic fibrosis, ionic-complex nanoparticles, Mn-porphyrin, retinoic acid, T_1 contrast MR imaging

1 | INTRODUCTION

Magnetic resonance (MR) contrast agents affect the spin–lattice (longitudinal, T_1) and spin–spin (transverse, T_2) relaxation times of protons, enhancing the spatial and temporal resolution of diagnostic MR imaging.[1,2] Among the paramagnetic metal ions with an unpaired electron, gadolinium (III) has been successfully introduced into clinical use as an MR contrast agent, showing a sufficient magnetic moment and a short relaxation time.[3,4] However, gadolinium (III), an exogenous element in the human body, should be used in the chelated form because of its safety issues.[5,6] Free gadolinium released from the chelates cause serious toxicity in the body.[7,8] Manganese, iron, and copper ions have been tried as attractive alternatives because these metals are abundant in the human body.[9,10] Currently, Teslascan® (manganese (II)-dipyridoxal diphosphate) for liver-specific T_1 contrast and LumenHance® (manganese (II) chloride) and FerriSeltz® (ferric ammonium citrate) for bowel imaging are clinically available.

Hoa Phuong Tran and Yixin Jiang contributed equally to this work.

The manganese porphyrins are another potential candidate for MR contrast agents. The multifunctional properties (i.e., tumor affinity, MR sensitivity, fluorescence, and photodynamic activity) of manganese porphyrins have attracted much attention and led to their clinical development.[11-14] Specifically, manganese (III)-tetraphenylporphyrin-sulfonate ($MnTPPS_4$) has been studied in various ways because $MnTPPS_4$ localizes in tumors more selectively, shows high MR relaxivity, and forms extraordinarily stable chelation complexes.[15,16] However, its further development has essentially stopped because the effective dose for contrast is only around fivefold lower than the LD_{50} of $MnTPPS_4$. Fortunately, currently developing nanotechnologies have attenuated such concerns. Mn-porphyrins in nano-form have been shown to be not only much more efficient MR contrast agents but also safer. Pan et al encapsulated Mn (III)-protoporphyrin with biotin-conjugated PEI self-assembling micelles for fibrin-targeted T_1 contrast imaging.[17] Their system preferentially accumulated in the fibrin clot area, enabling higher T_1 contrast. Zhang et al reported their development of dipicolylamine conjugated-$MnTPPS_4$ with dual imaging modalities (i.e., MRI and fluorescence) and achieved markedly enhanced T_1 contrast in the brain hippocampus with their use.[18]

Here, we selected $MnTPPS_4$ as a potential contrast agent for liver fibrosis detection. Interestingly, $MnTPPS_4$ is a negatively charged T_1-contrast agent which can form ionic-complex with cationic polymers.[14] And chitosan (CS) is a positive-charged biopolymer that has been used as an efficient drug delivery carrier. Ionic-complex formation of the positive-charged CS with negatively charged materials such as nucleotides have been reported several times.[19]

For the hepatic fibrosis-specific targeting design, we introduced retinoic acid (RA) to CS polymer. Retinoids are small lipophilic molecules that regulate gene transcription by binding to nuclear receptors known as retinoic acid receptors (RARs) and retinoid X receptors (RXRs) of liver.[20]

Here, we fabricated $MnTPPS_4$/retinoic acid-chitosan ionic-complex nanoparticles (MRC NPs) for noninvasive diagnostic T_1 contrast imaging of hepatic fibrosis. The nanoparticle formation was assessed by TEM imaging. The in vitro properties of MRC NPs (i.e., particle size, release of Mn, cellular cytotoxicity, and uptake by hepatocytes) were evaluated. Furthermore, the in vitro and in vivo MR imaging properties (T_1 relaxivity and MR contrast in a fibrosis rat model) were evaluated, and tissue distribution in mice was assessed.

2 | MATERIALS AND METHODS

2.1 | Preparation of MRC nanoparticles

In this study, RA (AK Scientific, Inc., Union City, CA) was selected as the hydrophobic core-forming material for chitosan (CS, m.w; 5 kDa, degree of deacetylation; 93%) nanoparticles.[21,22] Conjugation of RA on chitosan was performed as follows: 20 μmol RA was dissolved in 8 ml anhydrous DMSO (Sigma-Aldrich), followed by the addition of 1.1 equivalents of 1-ethyl-3-(3-dimethylaminopropyl)carbodiimide (EDC, Sigma-Aldrich, St. Louis, MO) and 4 equivalents of *n*-hydroxysuccinimide (NHS, Sigma-Aldrich, St. Louis, MO). The mixture was stirred at room temperature (20°C) for 30 min. CS (10 μmol) was dissolved in 20 ml of 1% acetic acid, followed by slow addition of 60 ml of DMSO. The RA solution was added gradually to the chitosan solution under magnetic stirring, and the mixture was then stirred at room temperature overnight. Then, a solution of 30 mg of $MnTPPS_4$ (Frontier scientific Inc., Logan, UT) in 10 ml of distilled water was added gradually under magnetic stirring. The resulting MRC was dialyzed using a dialysis tube with a molecular weight cutoff of 12–14 kDa (Spectrum®, Rancho Dominquez, CA), first against 80% ethanol solution for 1 day to remove free RA, then against 1% acetic acid solution for 1 day to remove free chitosan, and finally against distilled water for 1 day to remove free $MnTPPS_4$. After recovery, the sample was centrifuged at 3000 rpm for 30 min, and the supernatant was filtered with a 0.45 μm syringe filter. Synthesized MRC NPs were concentrated using an Amicon Stirred Ultrafiltration Cell (Merch Millipore, Billerica, MA) and then lyophilized (FreeZone 4.5, Labconco, Kansas, MO).

For the control studies, non-targeting $MnTPPS_4$/chitosan ionic-complex nanoparticles (MC NPs), fluorescein-labeled NPs (FITC-MRC NPs and FITC-MC NPs) were prepared (refer to Supporting Information).

2.2 | In vitro characterization of MRC nanoparticles

The conjugation of RA on chitosan was confirmed via ^{1}H-NMR (Varian Unity Inova 400 Mhz, Varian Inc, Palo, CA). The size distribution and zeta-potential of NPs were measured using the Zetasizer instrument (Nano-ZS90, Malvern Instruments, UK). NPs were dispersed in distilled water and assessed using a 90° scattering angle at 25°C. To observe the morphology of NPs, a drop of a concentrated sample solution was placed onto a carbon-coated, 200 square mesh copper grid and negatively stained with 1 drop of 2% phosphoric acid hydrate solution. The dried copper grids with NPs were examined under an H-7500 TEM (Hitachi, Japan). The Mn content of NPs were estimated using inductively coupled plasma-optical emission spectrometry (ICP-OES, Optima-7300DV, PerkinElmer Ltd., Co., Waltham, MA).

2.3 | In vitro release study

The in vitro release profiles of $MnTPPS_4$ from MRC NPs in various solutions (DI water, 0.9% NaCl, 10% FBS-media) were assessed. The NP solution (200 μl) was placed in a dialysis tube (GeBAflex-tube, MWCO 6–8 kDa, Gene Bio-Application Ltd., Israel), and the tube was immersed in 5 ml of distilled water, 0.1 M NaCl, or RPMI 1640 media containing 10% fetal bovine serum (FBS) and gently shaken at 37°C in a shaking incubator at 100 rpm. At predetermined time points, a sample of the solution was collected, and an equivalent amount of fresh solution was added to replace the collected sample. The $MnTPPS_4$ concentrations were determined using UV–Vis spectroscopy (U-2900, Hitachi, Japan).

2.4 | Cell culture

Hep3B (human hepatocellular carcinoma cell line) was obtained from the Korean Cell Line Bank (KCLB, Seoul, Republic of Korea) and incubated in RPMI-1640 medium (Gibco®, Invitrogen). Hepatic stellate cells (HSCs) and hepatocytes were isolated from the liver of Sprague–Dawley rats using in situ liver perfusion and a conventional density gradient centrifugation method and were cultured in Dulbecco's modified Eagle medium (DMEM, Gibco®, Invitrogen).[23] All culture media contained 10% FBS and 1% antibiotics, and all cells were incubated at 37°C in a 5% CO_2 humidified atmosphere.

2.5 | Estimation of cytotoxicity

Cells were seeded at a density of 2×10^3 cells/well in 96 well plates for Hep3B cells and 1×10^4 cells/well in 48 well plates for HSCs and hepatocytes. The established cell lines were incubated with MRC NPs over a concentration range of 0.01–0.5 μM as the concentration of Mn in NPs for 24 hr. Cytotoxicity was assayed using CellTiter-Glo® luminescent cell viability assay kit (Promega Co., Madison, WI). After 24 hr of incubation, cells were rinsed with PBS and treated with CellTiter-Glo® in a fresh culture medium for 30 min. Luminescence was measured using a plate reader (VICTOR® Multilabel Plate Reader, PerkinElmer, Walthamma, MA).

2.6 | Cellular uptake study

HSCs were seeded at a density of 1×10^6 cells/well on 22 × 22 mm glass cover slips placed in six well plates and incubated. When the cells reached 80% confluence, they were washed with fresh medium and incubated with fluorescein-labeled $MnTPPS_4$ chitosan NPs (FITC-MC NPs) or FITC-MRC NPs at a concentration of 10 μg $MnTPPS_4$ per ml for 2 hr. Then, the HSCs were washed twice with cold PBS, fixed with 4% paraformaldehyde, permeabilized with 0.5% Triton X-100 for 10 min, stained with DAPI (4′,6-Diamidino-2-phenylindole dihydrochloride, Vector Laboratories, Inc., Burlingame, CA), and mounted (VECTASHIELD HardSet™ mounting medium) for microscopic observation. The cellular uptake of NPs was measured at an excitation wavelength of 340 nm for DAPI, 414 nm for FITC, or 530 nm for $TPPS_4$, respectively, using a TCS SP5 II Dichroic/CS confocal microscope (Leica Microsystems GmbH, Wetslasr, Germany).

2.7 | In vitro estimation of T_1 relaxivity of MRC nanoparticles

The MR relaxivity of MRC NPs was measured. The concentration of Mn ions was measured using ICP-OES, and the T_1-contrast effect of MRC NPs according to Mn concentration (0–0.6 mM as Mn^{2+}) was evaluated. The r_1 relaxivity, defined as $1/T_1$ with units of s^{-1}, of the MRC NP solutions was measured at room temperature using a PharmaScan 7.0 T Preclinical MRI system (Bruker Co., MA). In vitro MR phantom imaging was performed in the same way. Solutions of $MnTPPS_4$ or MRC NPs with Mn concentrations of 0, 12.5, 25, 50, 75, and 100 μM were placed in 24 well plates and examined on a horizontal MRI scanner using a quad knee coil. MR images were analyzed using ImageJ software with the following conditions: spin echo, TR = 400 ms, and TE = 25, 50, 100, and 200 ms.

2.8 | Hepatic fibrosis rat modeling

All animal studies were approved by the Institutional Animal Care and Use Committee (IACUC) of Inha University. Male Sprague–Dawley rats (OrientBio, Korea) weighing between 250 and 300 g were selected for the study.

Rats received an intraperitoneal injection of dimethylnitrosamine (DMN, Sigma-Aldrich, St. Louis, MO) in 1-ml doses (diluted 1:100 with 0.15 M sterile NaCl) per 100 g body weight.[24,25] DMN injections were given on three consecutive days of each week for 4 weeks. The development of hepatic cirrhosis was monitored using histological assays of control rats under the same treatment. When hepatic fibrosis was established, the DMN-administered rats were introduced to the MR imaging study. At the end of MR imaging, rats were sacrificed under ketamine anesthesia and their livers were excised and weighed. The liver specimens were immediately fixed in 10% neutral buffered formaldehyde for histochemical studies.

2.9 | In vivo MR imaging study for hepatic fibrosis animal models

The hepatic fibrosis-induced rats were anesthetized and scanned using a 1.5 T MR scanner (Signa Excite; GE Healthcare, Milwaukee, WI) with a quad wrist coil. MRC NPs were introduced via tail vein injection at a dose of 25 μmol Mn/kg (102 mg/kg of MRC NPs). Rats were scanned 1, 30, 60, and 120 min after an administration. The pre- and post-contrast T_1-weighted images were acquired using the following parameters: spin echo, TR = 400 ms, TE = 10 ms, and slice thickness = 3.0 mm. The signal intensity (SI) of the hepatic lobe (the region of interest; ROI) was determined using Onis™ viewer. Signal intensities of ROIs are presented as contrast enhancement (CE), which was calculated using the following equation[26]:

$$CE\,(\%) = (SI_{post} - SI_{pre})/SI_{pre} \times 100.$$

2.10 | Plasma pharmacokinetic study of MRC nanoparticles

Male Sprague–Dawley rats (OrientBio, Korea) weighing between 250 and 300 g were selected for the pharmacokinetic studies. MRC NPs were intravenously injected via the tail vein injection. The injection dose was 30 mg/kg of free $MnTPPS_4$, which was equivalent with

27 μmol Mn/kg. Blood samples were collected from the femoral artery at predetermined time intervals and centrifuged for analysis. The acquired plasma samples were subjected to ICP-OES to determine the Mn concentration.

2.11 | Hepatic tissue distributions of MRC nanoparticles

The tissue distribution of MRC NPs was assessed using male ICR mice (weighing 25–30 g, OrientBio, Korea). The FITC-MRC NPs were intravenously injected into the tail vein of mice at the dose of 30 mg/kg free $MnTPPS_4$ (27 μmol Mn/kg). FITC-MC NPs were used as a control. The mice were sacrificed at 20 min, 60 min, 6 hr, 18 hr, and 72 hr after injection, the liver was recovered, fixed with 10% neutral formalin for 1 day, washed with PBS, and immersed in a 30% sucrose solution for 3 days. The fixed livers were embedded in OCT compounds, frozen on dry ice, and cryo-sectioned (~7 μm). The tissue slides were mounted with DAPI-containing mounting medium (VECTASHIELD® Hard Set™ Mounting Medium with DAPI, Vector Laboratories, Inc., Burlingame, CA). Slides were imaged at an excitation wavelength of 488 nm using a TCS SP5 II Dichroic/CS confocal microscope (Leica Microsystems GmbH, Germany).

2.12 | Statistical analysis

Data are presented as the mean ± standard deviation (*SD*). All statistical analyses were conducted using SPSS (11.0 version) software. Data are presented as the mean ± standard deviation (*SD*). Statistical differences were evaluated with student *T*-test. The difference was considered significant when $p < .05$ (*), $p < .01$ (**) and $p < .001$ (***). Statistical analyses were conducted using SPSS Statistics software (IBM Co., Armonk, NY).

3 | RESULTS AND DISCUSSION

3.1 | Synthesis and characterization of MRC nanoparticles

Retinoic acid-chitosan conjugates were synthesized via amide bond formation mediated by EDC and NHS. The negatively charged $MnTPPS_4$ then interacted with chitosan through electrostatic interactions. Consequently, they underwent molecular self-assembly to form ionic-complex nanoparticles between positively charged chitosan and negatively charged $MnTPPS_4$. Hydrophobic RA molecules, conjugated with CS, works as core forming agent, as shown in Scheme 1a. Thus, we hypothesize that the synthesized MRC NPs will preferentially accumulate on the RA receptor of hepatic stellate cells and allow the T_1 contrast MR imaging of hepatic fibrosis nodules (Scheme 1b).

The conjugation of retinoic acid-chitosan was characterized by ^{1}H-NMR. The observed signal at 5.5–6.5 ppm indicated the presence of RA, whereas the proton signals of chitosan were observed at 2.8–4.0 ppm (Figure 1a).[27] Freshly prepared MRC NPs remained well dispersed in an aqueous solution at room temperature for over a month, indicating that these particles were stable for this period of time (data not shown). As shown in Figure 1b, the hydrodynamic diameter of MRC NPs was around 100–600 nm. However, the size of MRC NPs, observed under a TEM (Figure 1c), was around 100–200 nm and much smaller than those of hydrodynamic diameter. Swelling in the aqueous phase with resulting an increase particle size is one of typical properties of ionic-complex nanoparticles. These TEM images and size distribution data are highly correspondent with previously reported ionic-complex nanoparticles.[28,29]

3.2 | In vitro release of $MnTPPS_4$

The release of $MnTPPS_4$ from the MRC NPs was estimated in media (10% FBS), saline (0.1 M NaCl), and distilled water (DW; Figure 2). The release profiles indicated that Mn was released from the MRC NPs in a controlled manner for up to 24 hr. In saline or diluted FBS solution, 50% of the $MnTPPS_4$ was released within 12 hr, with complete release within 24 hr. The release of $MnTPPS_4$ in distilled water was less than 10%. As was mentioned, $MnTPPS_4$ is entrapped by chitosan via ionic interactions, and their charges suggested that $MnTPPS_4$-chloride exchange between the MRC NPs and release medium was a key factor for $MnTPPS_4$ release.[30] Moreover, RA was introduced to not only provide a targeting moiety but also serve as a core-forming hydrophobic domain; thus, it is possible that the formed hydrophobic core prevented the rapid dissociation of $MnTPPS_4$.

In the clinical field, most liver MR imaging, especially gadolinium (Gd)-based MR imaging, is performed 10–60 min after an injection of contrast agents. Gadopentetate dimeglumine (Gd-DTPA, Magnevist®, Bayer Schering Pharma AG), gadodiamide (Gd-DTPA-BMA, Omniscan®, GE Healthcare), and gadobutrol (Gd-DO3A-butrol, Gadovist®, Bayer Inc.) are frequently used in liver MR imaging. However, these agents do not allow a sufficient time for delayed hepatic imaging, because only 2–4% of dose accumulates in the liver and is rapidly excreted. Therefore, the extended MR time window over several hours which allows more flexible and reliable MR imaging may offer many clinical benefits. In these reasons, development of new hepatocyte-specific MR agent is major interests of science.[31,32]

Our study showed around 70% of $MnTPPS_4$ released during the 24 hr of release study. We are supposing the prolonged release of $MnTPPS_4$ may offer the prolonged diagnostic time window which could give a high quality of images and patients convenience.

3.3 | Cytotoxicity and cellular uptake of MRC NPs

The cytotoxic effects of MRC NPs on the Hep3B cell line, hepatocytes, and HSCs were assessed over the concentration range of Mn in MRC NPs 0.01–0.5 μM, and the results are shown in Figure 3. Compared to control, the various concentrations of MRC NPs did not show any notable cytotoxicity against any of the cells. Cheng and his

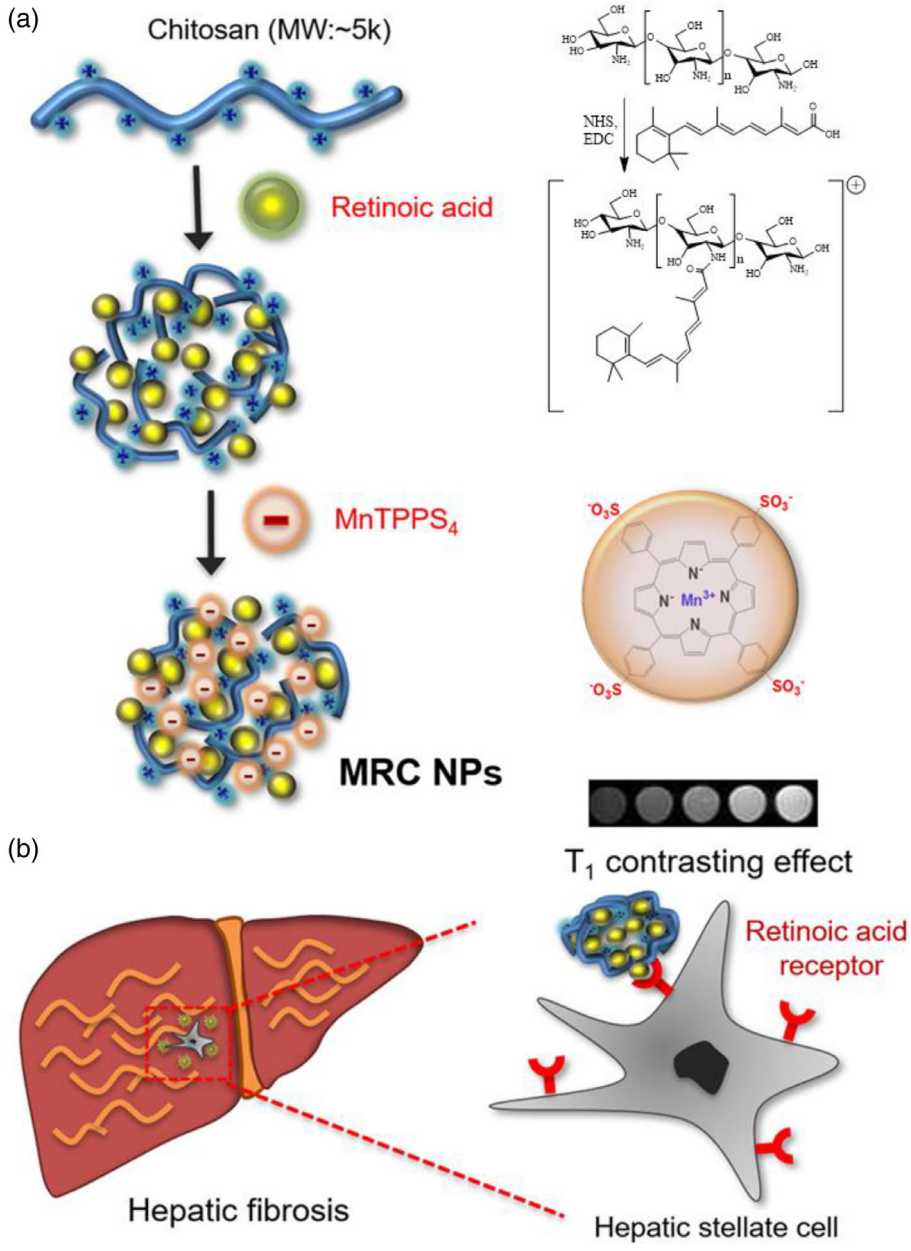

SCHEME 1 Representative schematic diagrams of (a) the fabrication of MRC NPs. MRC NPs were formed based on ionic complex between positive charged retinoic acid-chitosan conjugates and negative charged $MnTPPS_4$. (b) Binding of MRC NPs to retinoic acid receptor of hepatic cells and phantom T_1 contrast effect of MRC NPs. Hepatic stellate cells overexpress retinoic acid receptors during the development of the hepatic fibrosis

research group reported that $MnTPPS_4$ at 0.2 mM of concentration does not induced any cytotoxicity against human breast cancer cell lines (MDA-MB-231, MCF-7, and ZR-75-1).[14] Generally, chitosan is regarded to be biocompatible; however, polycations usually exhibit cytotoxicity against cells, and there have been some reports of the cyto- and tissue-toxic effects of chitosan.[33] The polycationic amines of chitosan were chemically conjugated with RA, which might have reduced the cytotoxicity of MRC NPs.

HSCs were treated with FITC-labeled NPs (FITC-MC NPs and FITC-MRC NPs) at a concentration of 0.001 μM for 2 hr, and the extent of uptake was determined using confocal laser microscopy. Figure 4 presents confocal images of the cells treated with $MnTPPS_4$, FITC-MC NPs, and FITC-MRC NPs. The specific uptake of $MnTPPS_4$ (red fluorescence) was observed in cells treated with $MnTPPS_4$ and FITC-labeled NPs in Figure 4a–c, respectively. Green fluorescence, generated from FITC-labeled NPs, was observed in Figure 4b,c. Generally, the strength of green and red fluorescence was much higher in FITC-MRC NPs treated cells (Figure 4c,d). Co-localization of green and red fluorescence, observed in Figure 4d, suggests that the RA-conjugated NPs undergo RA receptor-mediated endocytosis.

3.4 | In vitro T_1 relaxivity of MRC NPs

To evaluate the T_1 relaxivity and T_1 contrast properties of MRC NPs, samples of MRC NPs and $MnTPPS_4$ were prepared in 24 well plates and analyzed with a 7.0 T horizontal scanner, and the images were processed using ImageJ software. At the same Mn concentration, MRC NPs showed an enhanced T_1 contrast effect compared to that of $MnTPPS_4$ (Figure 5a). The longitudinal relaxation rates (r_1) of MRC

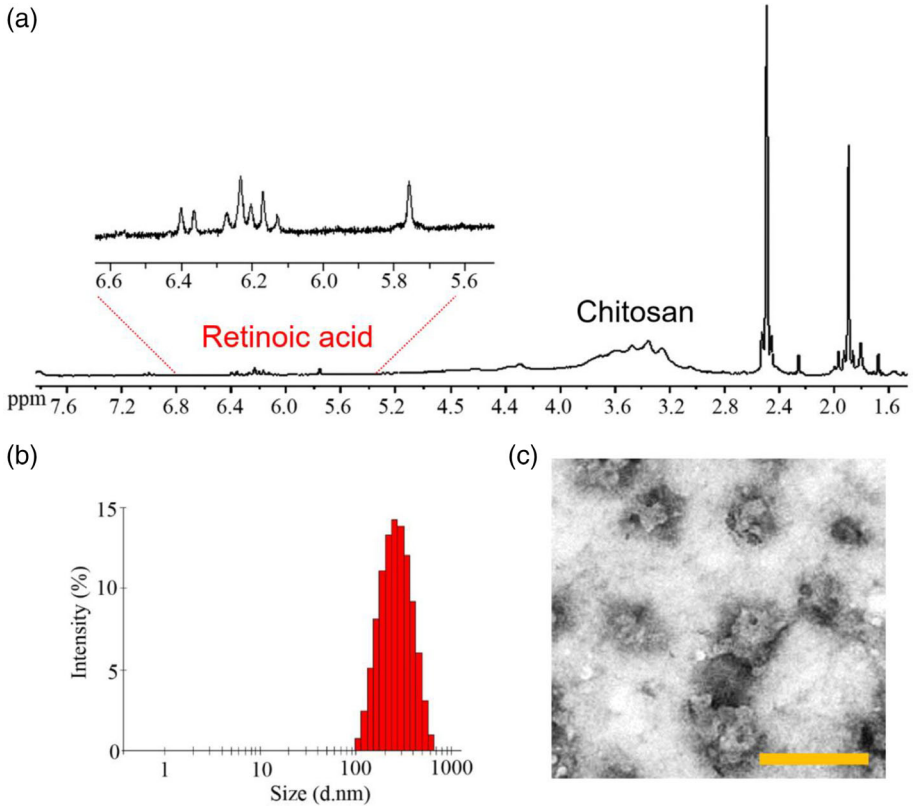

FIGURE 1 Characterization of MRC NPs. (a) ^{1}H NMR of retinoic acid-chitosan conjugate polymer. The observed signal at 5.5–6.5 ppm was indicated of RA, whereas proton signals of chitosan showed at 2.8–4.0 ppm. (b) Hydrodynamic size distribution of MRC NPs. (c) TEM image of MRC NPs (scale bar = 200 nm)

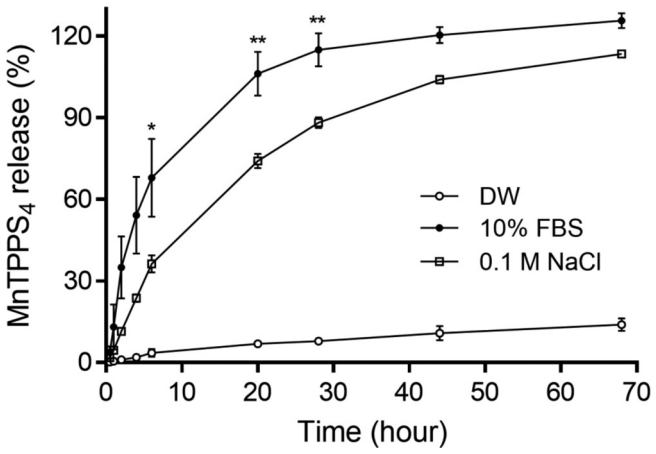

FIGURE 2 In vitro release profile of $MnTPPS_4$ from MRC NPs (mean ± *SD*, $n = 6$). Statistical analysis was performed between data of ●; 10% FBS and ■; 0.1 M NaCl (**$p < .05$, *$p < .1$). Release rate of $MnTPPS_4$ increased in biological fluidic media, because of competitive ion exchanges

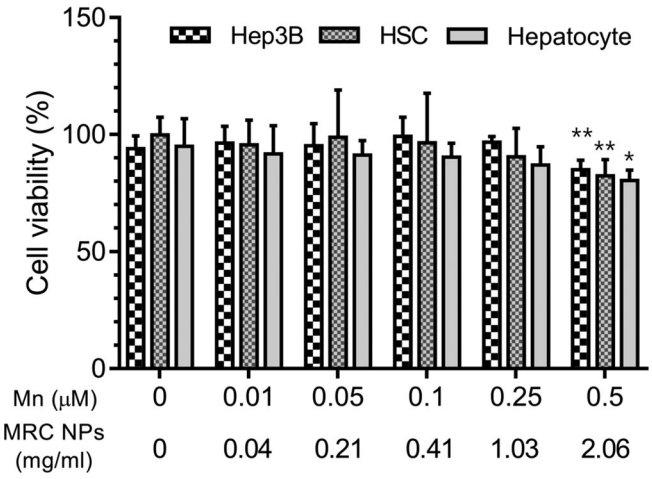

FIGURE 3 Cell viability of Hep3B, HSC and hepatic primary cells after MRC NPs treatment. MRC NPs did not show any significant cytotoxicity against the hepatic cells up to 1.0 mg/ml concentration (mean ± *SD*, $n = 6$, **$p < .05$, *$p < .1$)

NPs were compared with those of $MnTPPS_4$ over a range of Mn concentrations (0–0.6 mM as Mn^{2+}) using a PharmaScan 7.0 T Preclinical MRI system (Figure 5b). As shown in Figure 5b, $MnTPPS_4$ capped by MRC NPs had an r_1 value ($r_1 = 6.772\ mM^{-1}\ s^{-1}$) that was two times higher than that of $MnTPPS_4$ itself ($r_1 = 3.242\ mM^{-1}\ s^{-1}$). The higher T_1 relaxivity indicated that MRC NPs would produce brighter MR images than $MnTPPS_4$. Therefore, these results indicate that MRC NPs have the potential for MRI contrast agents.

3.5 | In vivo T_1 contrast MR imaging of hepatic fibrosis in rat models

MR images were taken prior to the injection of MRC NPs and at 1, 30, 60, and 120 min post-injection. Before the systemic administration of MRC NPs, it was difficult to differentiate between healthy liver and fibrotic nodules. However, after the administration of MRC NPs, the T_1 contrast increased approximately 15% 1 min after the

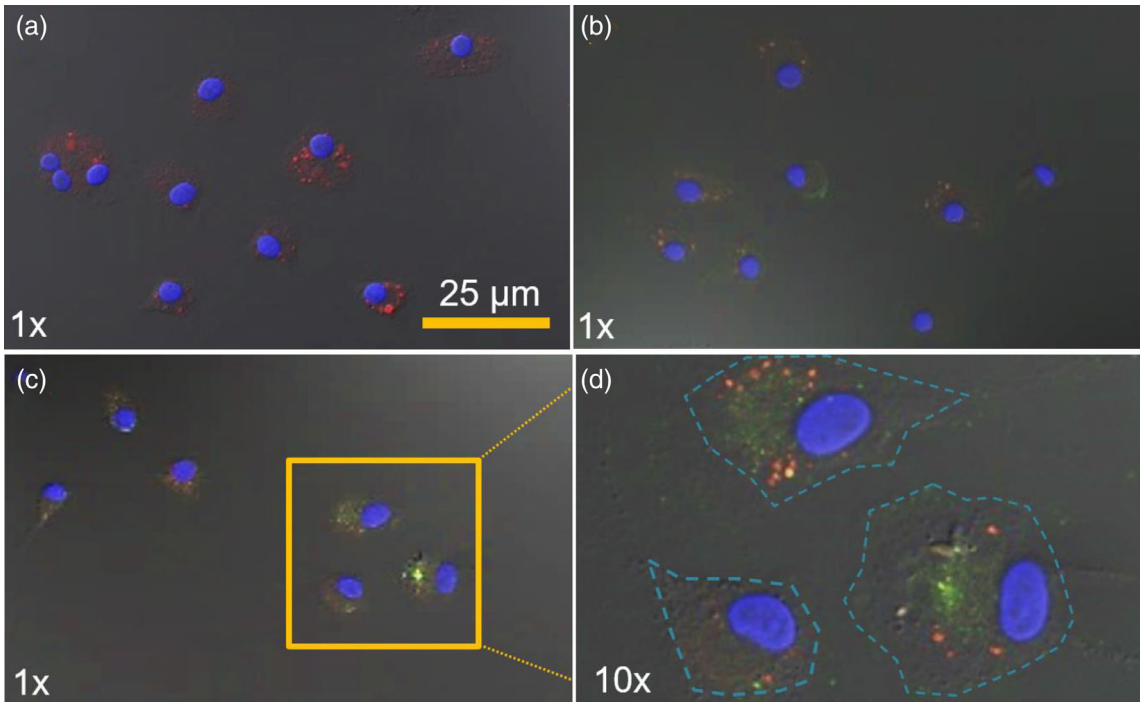

FIGURE 4 Hepatocyte uptake of FITC-MRC NPs and FITIC-MC NPs (blue: DAPI, green: FITC, red: $MnTPPS_4$). Cells are recovered and observed after 2 hr of incubation. (a) $TPPS_4$-treated HSC. (b) FITC-MC NPs treated HSC. (c and d) FITC-MRC NPs treated HSC

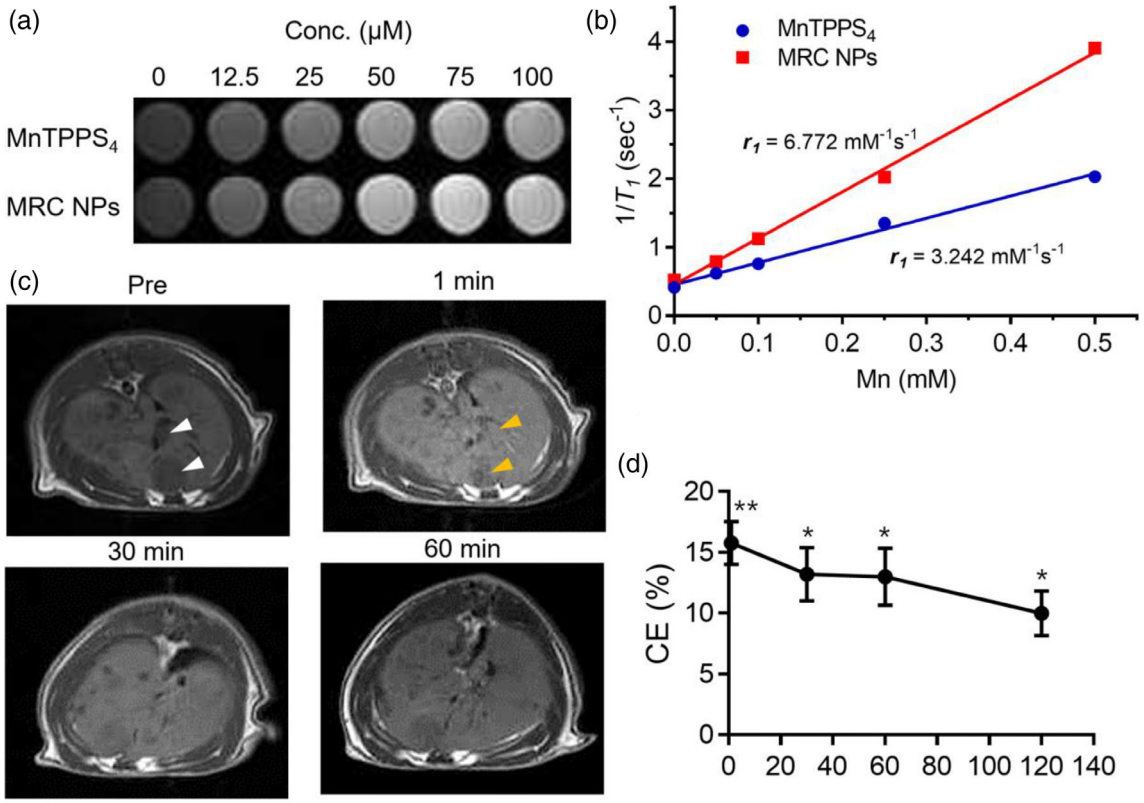

FIGURE 5 (a) T_1 contrast effect of MRC NPs in phantom study. (b) Longitudinal relaxation rates of MRC NPs and MnTPPS4. (c) In vivo T_1 contrast MR images after an intravenous injection of MRC NPs. (d) Contrast enhancement (CE, %) of ROI. ROI is selected from several points of hepatic lobes. Statistical analysis of CE was performed between each post-MR imaging and pre-MR imaging (mean ± *SD*, $n = 6$, $^{**}p < .05$, $^{*}p < .1$)

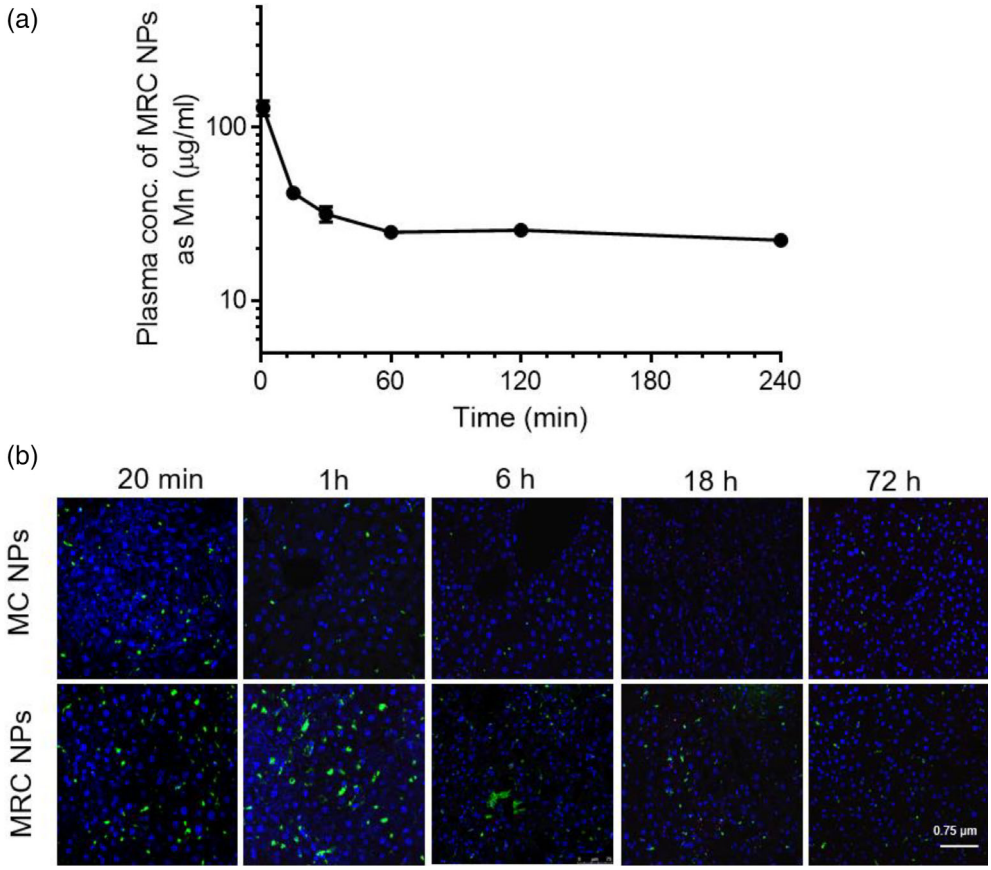

FIGURE 6 Plasma and hepatic tissue distribution of MRC NPs. (a) Plasma concentration-time curve of MRC NPs. The plasma concentration of MRC NPs (analyzed as concentration of $MnTPPS_4$) decreased rapidly for 10 min after an injection and then maintained over 20 μg/ml up to 240 min. (b) Fluorescence histology images of mouse liver tissues after an intravenous injection of FITC-MC NPs and FITC-MRC NPs (scale bar = 75 μm) with the green fluorescence of FITC and the blue color of DAPI. MRC NPs more highly accumulate and stay longer in hepatic tissues than MC NPs

administration of MRC NPs (Figure 5c; yellow arrowhead). The targeting effect was maintained up to 120 min post-injection, as depicted in Figure 5c,d. In addition, twofold higher contrast enhancement was observed against the normal mouse model (Figure S2).

Liver fibrosis is a hallmark of chronic liver disease resulting from chronic hepatic inflammation, such as alcoholic or viral hepatitis. Liver fibrosis is characterized by histological changes in the normal hepatic architecture with fibrotic nodules. Liver fibrosis may progress to cirrhosis, which constitutes the most important risk factor for HCC. Magnetic resonance (MR) imaging has now become the standard noninvasive imaging tool for use in the diagnosis of liver fibrosis. Hence, various MR imaging techniques for the diagnosis, staging, and monitoring of fibrosis nodules that may progress to invasive carcinoma have been studied.[34-36] For the hepatic fibrosis-targeted MR imaging, various modalities have been studied via chemical conjugation with the imaging probes such as Gd chelators or superparamagnetic iron oxide nanoparticles (SPIOs).

Caravan and his research group reported molecular MR imaging of liver fibrosis.[37] Gd based-collagen targeted probe (EP-3533) showed very marginal contrast enhancement in the dynamic MR imaging against CCl_4-treated mouse model. Recently, fibrosis-related collagen disposition related molecular targets, such as disulfide-bridged cyclic peptides and extracellular allysine, are developed for organ fibrosis imaging.[38] However, reliable and prognostic MR imaging of hepatic fibrosis is still clinical issues.[39]

In this study, we employed RA as an HSC-targeting modality. Approximately 70% of the retinoids in the body are stored in the liver. And especially, activated HSCs overexpress the RA receptor in the developmental stage of hepatic fibrosis.[40] The uptake of retinoic acid by the liver parenchyma, especially by HSCs, is greatly increased in disease states (hepatocellular carcinoma; HCC or cirrhosis).[25,27,41] So, RA has been abundantly studied for hepatic targeting and therapeutic delivery design. RA was encapsulated in polymeric scaffolds (hydrogels, nanofibers), nanoparticles (liposomes, micelles, polymeric, dendrimers), microparticles.[42-44] The carboxylic acid of RA can interact electrostatically with the amine group located in the polymer. Regarding chemical interaction, RA is conjugated to the nanoparticle through biodegradable ester amide or disulfide linkages. This bond is easily degraded in the specific pH conditions, proteases, or reducing agents that leading to release RA.[45] Sato et al designed vitamin A-coupled liposomes to deliver small interfering RNA (siRNA) to hepatic stellate cells. Their results were very promising, as the uptake of vitamin A-coupled liposomes by HS cells in a DMN-induced cirrhosis rat model was more than sixfold higher than with conventional liposomes.[46] Our data are also strongly supporting that RA targeting design, and its complex nanoparticles with T_1 contrast $MnTPPS_4$ enhanced the diagnostic contrast of animal hepatic fibrosis.

3.6 | Plasma and hepatic tissue distribution of MRC NPs

The plasma concentrations of MRC NPs at different time points are shown in Figure 6a. The Mn concentration, which represents the plasma MRC NPs content, quickly decreased for 10 min after the injection, and then maintained over 20 μg/ml up to 240 min. This

result corresponds with the long-lasting T_1 contrast effect of MRC NPs (Figure 5c,d).

In vivo hepatic tissue distributions of MRC NPs and MC NPs were compared after an intravenous injection of NPs into normal ICR mice. As expected, the MRC NPs had a greater fluorescence intensity than the MC NPs in the liver (Figure 6b). The maximal signal intensity was recorded at 60 min post-treatment, and the fluorescence signal was detected up to 72 hr. The liver tissue overexpress RA receptors, and RA-receptor-mediated endocytosis resulted in the accumulation of MRC NPs.[47] Combined with the result of Figure 6, the MRC NPs demonstrated a high potential MRI contrast agent for diagnostic hepatic fibrosis.

4 | CONCLUSIONS

In this study, we showed that MRC NPs performed successfully as a hepatic fibrosis targeting MRI contrast agent in both in vitro and in vivo experiments. We selected chitosan as a biocompatible nanocarrier and developed NPs conjugated with retinoic acid; the enhanced MRI contrast was achieved by the incorporation of $MnTPPS_4$ into the MRC NPs. The MRC NPs were found to have a monodisperse, spherical shape with favorable stability in PBS (pH 7.4) and no noticeable cytotoxicity. The MRC NPs showed MRI signal enhancement and preferential accumulation in the liver. The MRC NPs were retained in the liver for up to 72 hr. These results suggest that the MRC NPs have great potential as an MRI contrast agent for the early diagnosis of developing hepatic fibrosis and represent another valuable physiological tool for actively targeting the liver.

ACKNOWLEDGMENTS

This work was supported by the Basic Science Research Program and the Bio & Medical Technology Development Program of the National Research Foundation (NRF) funded by the Korean government (MOE and MSIT) (2020R1A2B5B02002377, 2018R1A6A1A03025523, and 2019M3E5D1A02069623). This work was also supported by INHA UNIVERSITY Research Grant.

DATA AVAILABILITY STATEMENT

The data that support the findings of this study are available within article.

REFERENCES

1. Xiao YD, Paudel R, Liu J, Ma C, Zhang ZS, Zhou SK. MRI contrast agents: classification and application (review). *Int J Mol Med*. 2016;*38*(5):1319-1326.
2. Jeong Y, Hwang HS, Na K. Theranostics and contrast agents for magnetic resonance imaging. *Biomater Res*. 2018;*22*(1):1-13.
3. Bellin MF. MR contrast agents, the old and the new. *Eur J Radiol*. 2006;*60*(3):314-323.
4. Clough TJ, Jiang L, Wong KL, Long NJ. Ligand design strategies to increase stability of gadolinium-based magnetic resonance imaging contrast agents. *Nat Commun*. 2019;*10*(1):1-13.
5. Caravan P, Ellison JJ, McMurry TJ, Lauffer RB. Gadolinium(III) chelates as MRI contrast agents: structure, dynamics, and applications. *Chem Rev*. 1999;*99*(9):2293-2352.
6. Yang CT, Chuang KH. Gd(iii) chelates for MRI contrast agents: from high relaxivity to "smart", from blood pool to blood–brain barrier permeable. *Med Chem Commun*. 2012;*3*(5):552-565. https://doi.org/10.1039/C2MD00279E.
7. Garcia J, Liu SZ, Louie AY. Biological effects of MRI contrast agents: gadolinium retention, potential mechanisms and a role for phosphorus. *Philos Trans R Soc A*. 2017;*375*(2107):1-28.
8. Jenjob R, Kun N, Ghee JY, et al. Enhanced conjugation stability and blood circulation time of macromolecular gadolinium-DTPA contrast agent. *Mater Sci Eng C*. 2016;*61*:659-664.
9. Wang J, Wang H, Ramsay IA, et al. Manganese-based contrast agents for magnetic resonance imaging of liver tumors: structure-activity relationships and Lead candidate evaluation. *J Med Chem*. 2018;*61*(19):8811-8824.
10. Bao Y, Sherwood JA, Sun Z. Magnetic iron oxide nanoparticles as T1 contrast agents for magnetic resonance imaging. *J Mater Chem C*. 2018;*6*(6):1280-1290. https://doi.org/10.1039/C7TC05854C.
11. Lyon RC, Faustino PJ, Cohen JS, et al. Tissue distribution and stability of metalloporphyrin MRI contrast agents. *Magn Reson Med*. 1987;*4*(1):24-33.
12. Mouraviev V, Venkatraman TN, Tovmasyan A, et al. Mn porphyrins as novel molecular magnetic resonance imaging contrast agents. *J. Endourol*. 2012;*26*(11):1420-1424.
13. Venter A, Szulc DA, Loai S, Ganesh T, Haedicke IE, Cheng HL. A manganese porphyrin-based T1 contrast agent for cellular MR imaging of human embryonic stem cells. *Sci Rep*. 2018;*8*(1):12129-12140.
14. Alhamami M, Cheng W, Lyu Y, Allen C, Zhang XA, Cheng HL. Manganese-porphyrin-enhanced MRI for the detection of cancer cells: a quantitative in vitro investigation with multiple clinical subtypes of breast cancer. *PLoS One*. 2018;*13*(5):1-17.
15. Yushmanov VE, Tominaga TT, Borissevitch IE, Imasato H, Tabak M. Binding of manganese and iron tetraphenylporphine sulfonates to albumin is relevant to their contrast properties. *Magn Reson Imaging*. 1996;*14*(3):255-261. https://doi.org/10.1016/0730-725X(95)02103-Z.
16. Klein AT, Rosch F, Coenen HH, Qaim SM. Labelling of manganese-based magnetic resonance imaging (MRI) contrast agents with the positron emitter 51Mn, as exemplified by manganese-tetraphenylporphin-sulfonate (MnTPPS4). *Appl Radiat Isot*. 2005;*62*(5):711-720.
17. Pan D, Caruthers SD, Hu G, et al. Ligand-directed nanobialys as theranostic agent for drug delivery and manganese-based magnetic resonance imaging of vascular targets. *J Am Chem Soc*. 2008;*130*(29):9186-9187.
18. Zhang XA, Lovejoy KS, Jasanoff A, Lippard SJ. Water-soluble porphyrins as a dual-function molecular imaging platform for MRI and fluorescence zinc sensing. *Proc Natl Acad Sci U S A*. 2007;*104*(26):10780-10785.
19. Maya S, Sarmento B, Lakshmanan VK, Menon D, Seabra V, Jayakumar R. Chitosan cross-linked docetaxel loaded EGF receptor targeted nanoparticles for lung cancer cells. *Int J Biol Macromol*. 2014;*69*:532-541.
20. Ulven SM, Natarajan V, Holven KB, Løvdal T, Berg T, Blomhoff R. Expression of retinoic acid receptor and retinoid X receptor subtypes in rat liver cells: implications for retinoid signalling in parenchymal, endothelial, Kupffer and stellate cells. *Eur J Cell Biol*. 1998;*77*(2):111-116.
21. Fattahi A, Golozar M-A, Varshosaz J, Sadeghi HM, Fathi M. Preparation and characterization of micelles of oligomeric chitosan linked to all-trans retinoic acid. *Carbohydr Polym*. 2012;*87*(2):1176-1184.
22. Cho CS, Cho KY, Park IK, et al. Receptor-mediated delivery of all trans-retinoic acid tohepatocyte using poly(L-lactic acid) nanoparticles

coated withgalactose-carrying polystyrene. *J Control Release*. 2001;77 (1–2):7-15.
23. Kim M, Yang SG, Kim JM, Lee JW, Kim YS, Lee JI. Silymarin suppresses hepatic stellate cell activation in a dietary rat model of non-alcoholic steatohepatitis: analysis of isolated hepatic stellate cells. *Int J Mol Med*. 2012;*30*(3):473-479.
24. Maeng JH, Lee DH, Jung KH, et al. Multifunctional doxorubicin loaded superparamagnetic iron oxide nanoparticles for chemotherapy and magnetic resonance imaging in liver cancer. *Biomaterials*. 2010;*31* (18):4995-5006.
25. Kim MK, Kim MA, Yim JH, Lee DH, Cho SK, Yang SG. Ramalin, an antioxidant compound derived from Antarctic lichen, prevents progression of liver fibrosis induced by dimethylnitrosamine (DNM) in rats. *Biochem Biophys Res Commun*. 2018;*504*(1):25-33.
26. Stiskal M, Schwickert HC, Demsar F, et al. Contrast enhancement in experimental radiation-induced liver injury: comparison of hepatocellular and reticuloendothelial particulate contrast agents. *J Magn Reson Imaging*. 1996;*6*(2):286-290.
27. Varshosaz J, Hassanzadeh F, Sadeghi H, Ghelich Khan Z, Rostami M. Retinoic acid decorated albumin-chitosan nanoparticles for targeted delivery of doxorubicin hydrochloride in hepatocellular carcinoma. *J Nanomater*. 2013;*2013*:1-12.
28. Ji N, Hong Y, Gu Z, Cheng L, Li Z, Li C. Fabrication and characterization of complex nanoparticles based on carboxymethyl short chain amylose and chitosan by ionic gelation. *Food Funct*. 2018;*9*(5):2902-2912.
29. Pilipenko I, Korzhikov-Vlakh V, Sharoyko V, et al. pH-sensitive chitosan-heparin nanoparticles for effective delivery of genetic drugs into epithelial cells. *Pharmaceutics*. 2019;*11*(7):317–332.
30. Chavanpatil MD, Khdair A, Patil Y, Handa H, Mao G, Panyam J. Polymer-surfactant nanoparticles for sustained release of water-soluble drugs. *J Pharm Sci*. 2007;*96*(12):3379-3389.
31. Yim H, Yang SG, Jeon YS, et al. The performance of gadolinium diethylene triamine pentaacetate-pullulan hepatocyte-specific T1 contrast agent for MRI. *Biomaterials*. 2011;*32*(22):5187-5194.
32. Semelka R, Helmberger T. Contrast agents for MR imaging of the liver. *Radiology*. 2001;*218*(1):27-38.
33. Chae SY, Jang MK, Nah JW. Influence of molecular weight on oral absorption of water soluble chitosans. *J Control Release*. 2005;*102*(2): 383-394.
34. Liu Y, Chen Z, Liu C, Yu D, Lu Z, Zhang N. Gadolinium-loaded polymeric nanoparticles modified with anti-VEGF as multifunctional MRI contrast agents for the diagnosis of liver cancer. *Biomaterials*. 2011; *32*(22):5167-5176.
35. Moon S, Yang SG, Na K. An acetylated polysaccharide-PTFE membrane-covered stent for the delivery of gemcitabine for treatment of gastrointestinal cancer and related stenosis. *Biomaterials*. 2011;*32*(14):3603-3610.
36. Ramalho M, Matos AP, AlObaidy M, Velloni F, Altun E, Semelka RC. Magnetic resonance imaging of the cirrhotic liver: diagnosis of hepatocellular carcinoma and evaluation of response to treatment - part 1. *Radiol Bras*. 2017;*50*(1):38-47.
37. Polasek M, Fuchs BC, Uppal R, et al. Molecular MR imaging of liver fibrosis: a feasibility study using rat and mouse models. *J Hepatol*. 2012;*57*(3):549-555.
38. Desogere P, Montesi SB, Caravan P. Molecular probes for imaging fibrosis and Fibrogenesis. *Chemistry*. 2019;*25*(5):1128-1141. https://doi.org/10.1002/chem.201801578.
39. Starkel P, Leclercq IA. Animal models for the study of hepatic fibrosis. *Best Pract Res Clin Gastroenterol*. 2011;*25*(2):319-333.
40. Haaker MW, Vaandrager AB, Helms JB. Retinoids in health and disease: a role for hepatic stellate cells in affecting retinoid levels. *Biochim Biophys Acta Mol Cell Biol Lipids*. 1865;*2020*(6):158674-158685. https://doi.org/10.1016/j.bbalip.2020.158674.
41. Yanagitani A, Yamada S, Yasui S, et al. Retinoic acid receptor alpha dominant negative form causes steatohepatitis and liver tumors in transgenic mice. *Hepatology*. 2004;*40*(2):366-375.
42. O'Leary C, O'Brien FJ, Cryan S-A. Retinoic acid-loaded collagen-hyaluronate scaffolds: a bioactive material for respiratory tissue regeneration. *ACS Biomater Sci Eng*. 2017;*3*(7):1381-1393.
43. Carpenedo RL, Bratt-Leal AM, Marklein RA, et al. Homogeneous and organized differentiation within embryoid bodies induced by microsphere-mediated delivery of small molecules. *Biomaterials*. 2009;*30*(13):2507-2515.
44. Huang H, Shi H, Liu J, et al. Co-delivery of all-trans-retinoic acid enhances the anti-metastasis effect of albumin-bound paclitaxel nanoparticles. *Chem Commun*. 2016;*53*(1):212-215.
45. Ferreira R, Napoli J, Enver T, Bernardino L, Ferreira L. Advances and challenges in retinoid delivery systems in regenerative and therapeutic medicine. *Nat Commun*. 2020;*11*(1):4265.
46. Sato Y, Murase K, Kato J, et al. Resolution of liver cirrhosis using vitamin A-coupled liposomes to deliver siRNA against a collagen-specific chaperone. Nat. *Biotechnol*. 2008;*26*(4):431-442.
47. Li Y, Wong K, Walsh K, Gao B, Zang M. Retinoic acid receptor beta stimulates hepatic induction of fibroblast growth factor 21 to promote fatty acid oxidation and control whole-body energy homeostasis in mice. *J Biol Chem*. 2013;*288*(15):10490-10504.

SUPPORTING INFORMATION

Additional supporting information may be found online in the Supporting Information section at the end of this article.

How to cite this article: Tran, H. P., Jiang, Y., Nguyen, P. H., Kim, J. J., & Yang, S.-G. (2022). Retinoic acid-conjugated chitosan/manganese porphyrin ionic-complex nanoparticles for improved T_1 contrast MR imaging of hepatic fibrosis. *Journal of Biomedical Materials Research Part B: Applied Biomaterials*, *110*(2), 382–391. https://doi.org/10.1002/jbm.b.34914